This is a repository copy of *Nanostructure of CaO-(Na2O)-Al2O3-SiO2-H2O gels revealed by multinuclear solid-state magic angle spinning and multiple quantum magic angle spinning nuclear magnetic resonance spectroscopy*.

White Rose Research Online URL for this paper:
http://eprints.whiterose.ac.uk/157832/

Version: Accepted Version

Nanostructure of CaO-(Na₂O)-Al₂O₃-SiO₂-H₂O Gels Revealed by Multinuclear Solid State MAS and MQMAS NMR

Brant Walkley[1,2†], Samuel J. Page[3†], Gregory J. Rees[3], John L. Provis[1], John V. Hanna[3]*

[1] Department of Materials Science and Engineering, The University of Sheffield, Sheffield S1 3JD, United Kingdom

[2] Department of Chemical and Biological Engineering, The University of Sheffield, Sheffield S1 3JD, United Kingdom

[3] Department of Physics, The University of Warwick, Coventry CV4 7AL, United Kingdom

[†] These authors contributed equally to this work. * Corresponding author. Email: j.v.hanna@warwick.ac.uk

Abstract

(Calcium,alkali)-aluminosilicate gel frameworks are the basis of modern cements and alkali-activated materials for sustainable infrastructure and radioactive waste immobilisation, and also find application in glass alteration, mineral weathering, and zeolite synthesis. Here, we resolve the nanostructure of these gels that dictates mass transport, solubility and mechanical properties. The key structural motifs comprising hydrous (calcium,alkali)-aluminosilicate gels are identified via ^{17}O, ^{23}Na and ^{27}Al 3QMAS and ^{29}Si MAS NMR spectroscopy of a novel class of stoichiometrically controlled ^{17}O-enriched multiphase gels. Increased Ca content promotes low-Al, high-Ca chain-structured "C-S-H-type" products exhibiting significant nanostructural ordering, low levels of chain crosslinking, predominant Ca coordination of non-bridging oxygen atoms, and an increase in proton association with CaO layers to form Ca-OH sites. Al substitution is identified in multiple sites in the silicate chains, including crosslinking, bridging and pairing tetrahedra. Increased Al content increases the proportion of crosslinking sites and gel disorder. The large increase in Si^{IV}-O-Al^{IV} sites increases the relative amounts of Na^+ and Al^V species charge-balancing AlO_4^- tetrahedra, formation of an additional disordered low-calcium, framework-structured alkali aluminosilicate ("N-A-S-H-type") gel, with high Al and Na content. Changes in bulk composition significantly alter the nanostructures of the C-S-H-type and N-A-S-H-type gels. Mean Si^{IV}-O-Al^{IV} bond angles for each type of Al^{IV} site environment are highly consistent, with compositional changes dictating the relative proportions of individual Al^{IV} species but not altering the local structure of each Al^{IV} site. These reveal the molecular interactions governing (calcium,alkali)-aluminosilicate gel nanostructure, which are crucial in controlling material properties and durability.

1. Introduction

(Calcium,alkali)-aluminosilicate gel frameworks have received significant academic and commercial interest in recent years due to their technological potential in applications such as glass alteration, mineral weathering, construction materials, zeolite synthesis and alkali-activated materials, among many others. This broad class of materials is formed by reaction of an alkaline or alkali-silicate solution with an aluminosilicate or calcium aluminosilicate precursor and characterised by a crosslinked, predominantly X-ray amorphous network[1-2].

The nanostructure of aluminosilicate gels is dictated by the alkali and alkaline earth cations present within the mix formulation, most commonly calcium and sodium, and is largely dependent on the amount of calcium present. Presence of Ca^{2+} results in formation of an aluminium-substituted calcium silicate hydrate (C-(A)-S-H) gel (which in the presence of Na^+ may also form a sodium- and aluminium-substituted calcium silicate hydrate (C-(N)-(A)-S-H) gel) with a tobermorite-like structure displaying ordering ranging from X-ray amorphous to low-crystallinity. Low Ca^{2+} content in the presence of Na^+ results in formation of a sodium aluminosilicate hydrate (N-A-S-H) gel framework with a highly polymerised, disordered pseudo-zeolitic structure[3]. Coexistence of both C-(A)-S-H and N-A-S-H gel frameworks, each with vastly different nanostructures, results in complex thermodynamic and chemical interactions which dictate phase and nanostructural evolution[4].

Understanding the chemical and physical parameters governing the phase and nanostructural evolution of these materials remains an important scientific challenge. In particular, the role of Al in forming and promoting crosslinking sites within C-(N)-A-S-H has been a key focal point. The presence of high contents of Al has been shown to greatly influence the gel nanostructure[4-5], dictating the formation and structural evolution of C-(N)-A-S-H and N-A-S-H gels as well as various additional reaction products, including hydrocalumite-like (AFm structured) layered double hydroxides which have significant implications for material strength and durability[6-7]. The relationship between the relative amounts of key network forming (Si, Al) and network modifying (Na^+, Ca^{2+}) cations has been shown to be very complex[4-5, 8].

The multi-phase nature of these crystallographically disordered and dynamic systems has caused significant difficulty in gaining detailed information regarding the atomic structure of C-(N)-A-S-H, C-A-S-H and N-A-S-H gels. Solid state magic angle spinning nuclear magnetic resonance (MAS NMR) spectroscopy investigations probing ^{27}Al, ^{29}Si and ^{23}Na nuclei in these materials have provided information about the coordination and connectivity of these atoms [9-13]. However, while studies utilising ^{17}O MAS NMR have yielded important structural information regarding a large variety of

zeolites, aluminosilicate and calcium aluminosilicate glasses[14-21], few have probed the hydrous gel structures using ^{17}O nuclei. The very low natural abundance (0.037%) of the NMR-active ^{17}O nucleus necessitates isotopic enrichment of samples[22-25] and has consequently limited the application of solid state MAS NMR experiments probing this nucleus in (calcium,alkali)-aluminosilicate gels. Significant line broadening occurs at practically achievable MAS rates due to the disordered structure of (calcium,alkali)-aluminosilicate gels. Additionally, quadrupolar nuclei (spin $I > 1/2$) such as ^{27}Al ($I = 5/2$), ^{17}O ($I = 5/2$) and ^{23}Na ($I = 3/2$) experience second order quadrupolar broadening which is not fully averaged by MAS. Consequently, spectroscopic data for these materials tend to be poorly resolved[26-27].

Recently, multiple quantum magic angle spinning (MQMAS) spectroscopy[26-27] probing half integer quadrupolar nuclei including ^{17}O, ^{23}Na, and ^{27}Al has been used to obtained high resolution NMR spectra of alkali aluminosilicate gels[22-23, 28-31], related reaction products[29, 32] and precursors[16] from which these gels can be synthesised. MQMAS achieves high resolution by partially averaging the fourth-order Legendre polynomial by conversion of symmetric multiple quantum coherence (pQ, $p = 3$, 5, 7, … for $p \leq 2I$) to the single quantum ($1Q$) detectable central transition, and plotting pQ and $1Q$ correlations in two dimensions[22]. Consequently, anisotropic second-order broadening can be removed from the multiple quantum dimension, leaving a spectrum which is dominated by the chemical shift. This enables chemical species with similar local structures and coordination environments, which would otherwise result in overlapping resonances in 1D MAS NMR spectra, to be resolved.

Standard processing of MQMAS spectra, using single-axial isotropic shearing (iso-shearing) in the indirect dimension, removes the second-order quadrupolar term and leaves the projection of the spectra onto the multiple quantum dimension axis as a pure function of isotropic variables such as the isotropic chemical shift (δ_{iso}) and the quadrupolar induced shift (δ_{QIS}), which may enable chemically distinct sites to be resolved in the multiple quantum (pQ) dimension[22, 28, 33-34]. However, the more recently introduced method of biaxial Q-shearing[22] in both the indirect and direct dimensions allows orthogonal separation of δ_{iso} from both δ_{QIS} and the quadrupolar coupling constant (C_Q), and is particularly useful for disordered materials which typically give MQMAS spectra displaying a distribution of chemical shift and quadrupolar parameters that can be difficult to interpret for identification of chemically distinct sites[22, 35].

Solid state MQMAS NMR has recently been used to probe ^{27}Al, ^{23}Na and ^{17}O nuclei within phase pure N-A-S-H in synthetic alkali-aluminosilicate gels, and to develop a molecular model describing the structure of the N-A-S-H gel framework in these materials[31]. This has provided an important platform from which to understand the physicochemical interactions within, and between, C-(N)-A-S-H, C-A-S-

H and N-A-S-H gel frameworks. Therefore, here we use ^{27}Al, ^{23}Na and ^{17}O MAS and 3QMAS NMR spectroscopy to examine the nanostructure in a newly-validated class of stoichiometrically controlled multiphase C-(N)-A-S-H, C-A-S-H and N-A-S-H gel frameworks[4, 36-37]. A range of shearing schemes are used to generate spectra broadened only by the isotropic chemical shift or by the quadrupolar interaction.

The key motifs which assemble to form the C-(N)-A-S-H, C-A-S-H and N-A-S-H gel frameworks are identified, and a detailed molecular description of the structure of these gels is developed, including Al substitution sites and bond angles within the gel. This is then used to examine the effect of variations in precursor composition on the nanostructure of these gels. Of particular interest are the local coordination and nearest-neighbour environments of the key network-forming Si, Al and O atoms, network-modifying Na and Ca atoms, and associated H_2O molecules. This structural description establishes a new depth of understanding of the molecular interactions governing the nanostructure of these gels, and how these interactions are controlled by precursor composition and mix formulation.

2. Experimental methods

2.1 Materials

The synthetic (calcium,alkali)-aluminosilicate gels used in this study were produced by alkali-activation of synthetic calcium aluminosilicate precursor powders, which had been synthesised using an organic steric entrapment solution-polymerisation method[36]. Gel cation ratios are outlined in Table 1. Full details of the sample synthesis procedure are provided in Supporting Information.

Table 1: Empirical formulae, elemental molar ratios and water/solid (w/s) mass ratios, of the reaction mixes

	Precursor	*Reaction mix*				
Sample	Empirical formula	Empirical formula	Ca/(Al+Si)	Al/Si	Na/Al	w/s
A	$0.800CaO \cdot SiO_2 \cdot 0.078Al_2O_3$	$0.771CaO \cdot SiO_2 \cdot 0.075Al_2O_3 \cdot 0.038Na_2O$	0.67	0.15	0.50	0.75
B	$1.214CaO \cdot SiO_2 \cdot 0.078Al_2O_3$	$1.15CaO \cdot SiO_2 \cdot 0.075Al_2O_3 \cdot 0.038Na_2O$	1.00	0.15	0.50	1.00
C	$0.709CaO \cdot SiO_2 \cdot 0.026Al_2O_3$	$0.704CaO \cdot SiO_2 \cdot 0.025Al_2O_3 \cdot 0.013Na_2O$	0.67	0.05	0.50	0.60
D	$1.104CaO \cdot SiO_2 \cdot 0.026Al_2O_3$	$1.05CaO \cdot SiO_2 \cdot 0.025Al_2O_3 \cdot 0.013Na_2O$	1.00	0.05	0.50	0.75

2.2 NMR spectroscopy

All ^{17}O, ^{23}Na and ^{27}Al MAS and 3QMAS data were obtained at 14.1 T using a Bruker Avance II+ spectrometer operating at a Larmor frequency of 156.2 MHz, 158.6 MHz and 81.26 MHz for ^{27}Al, ^{23}Na

and ^{17}O, respectively, and a Bruker 3.2 mm double air-bearing probe calibrated to yield a MAS frequency of 20 kHz for each experiment. ^{27}Al MAS spectra were acquired using a 1 µs selective (π/9) excitation pulse, a measured 1 s relaxation delay and a total of 4096 transients, while ^{27}Al 3QMAS experiments were acquired using a 4.5 µs non-selective triple quantum excitation pulse followed by a 1.5 µs non-selective conversion pulse and a selective 20 µs z-filter pulse. All ^{27}Al MAS and 3QMAS spectra are referenced to the secondary reference yttrium aluminium garnet ($\delta_{iso}(AlO_6)$ = 0.7 ppm with respect to 1.1 M $Al(NO_3)_{3\ (aq)}$ = 0 ppm). ^{23}Na MAS spectra were acquired using a 1 µs non-selective (π/4) excitation pulse, a measured 1 s relaxation delay and a total of 4096 transients, while ^{23}Na 3QMAS experiments were conducted using a 4.0 µs non-selective triple quantum excitation pulse followed by a 1.2 µs non-selective conversion pulse and a selective 20 µs z-filter pulse. All ^{23}Na MAS and 3QMAS spectra are referenced to solid sodium chloride as a secondary reference ($\delta_{iso}(NaCl_{(s)})$ = 7.2 ppm with respect to 1 M NaCl $_{(aq)}$ = 0 ppm). ^{17}O MAS spectra were acquired using a 1.75 µs non-selective (π/2) excitation pulse, a measured 1 s relaxation delay and a total of 2048 transients, while ^{17}O 3QMAS experiments were conducted using a 7.0 µs non-selective triple quantum excitation pulse followed by a 2.0 µs non-selective conversion pulse and a selective 17.5 µs z-filter pulse. All ^{17}O MAS and 3QMAS spectra are referenced to $H_2^{17}O$ at 0 ppm. All ^{29}Si MAS NMR data were obtained at 14.1 T using an Agilent VNMRS-600 spectrometer operating at a Larmor frequency of 119.14 MHz and a 4.0mm triple resonance bioMAS probe calibrated to yield a MAS frequency of 10 kHz for each experiment. All ^{29}Si MAS spectra were acquired using a 7 µs non-selective (π/2) excitation pulse, a measured 120 s relaxation delay and a total of 1024 scans, and were referenced to neat tetramethylsilane at 0 ppm. All 3QMAS spectra were processed using either TopSpin or NMRPipe[38] software. Spectral simulations were performed using DMFit[39-40] and the Czjzek Gaussian isotropic model[41]. All ^{29}Si MAS NMR data were processed using NMRPipe[38] and deconvoluted by fitting Gaussian peak profiles[39]. Full details of all processing and fitting procedures is provided in Supporting Information.

3. Results and discussion

3.1 ^{29}Si MAS NMR

A detailed discussion of the ^{29}Si MAS NMR data for these samples has been published previously[4, 36], however this data and the associated spectral deconvolutions are also presented here (Figure 1) to provide context for interpretation of the ^{27}Al MAS and 3QMAS NMR data discussed below. Each precursor comprises Q^2, Q^2(1Al), Q^3 and Q^3(1Al) sites within a depolymerised calcium silicate phase as well as smaller amounts of Q^4, Q^4(1Al) and Q^4(2Al) within a highly polymerised aluminosilicate phase[36]. Q^0 and Q^1 are also observed within low Al-containing precursors C and D and are attributed to dicalcium silicate (C_2S) and clinozoisite, respectively.

Alkali-activation of all precursors results in formation of six new Si environments indicated by peaks at approximately −79 ppm, −82 ppm, −85 ppm, −88 ppm and −94 ppm, attributed to Q^1, Q^2(1Al), Q^2, Q^3(1Al), and Q^3, respectively, within a C-(N)-A-S-H gel, with a degree of crosslinking occurring in each sample as evidenced by the Q^3 and Q^3(1Al) sites[4]. Spectral deconvolutions consistent with the structural constraints described by the CSTM for C-(N)-A-S-H gel products[42], and the thermodynamics of a statistical distribution of Si and Al sites within a Q^4 aluminosilicate network for N-A-S-(H) gel products[43], show the formation of an additional Al-rich N-A-S-H gel in samples containing higher nominal Al content. Formation of a new resonance at −76 ppm is also observed in each sample by both ^{29}Si MAS and ^{1}H-^{29}Si CP MAS NMR, and this resonance was tentatively attributed to Q^0 sites within the newly formed reaction product[4], although this site could not be clearly explained[4].
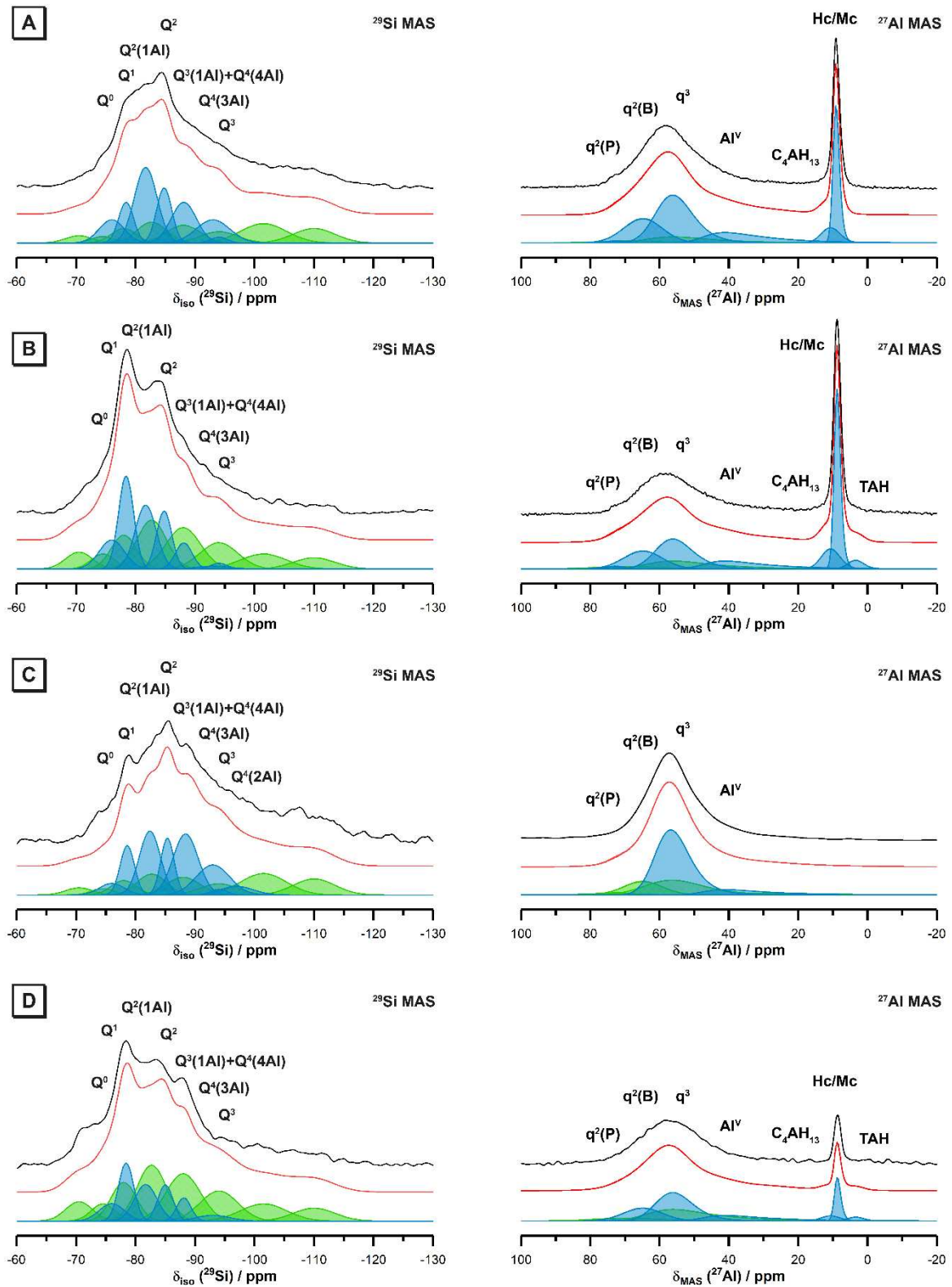
Figure 1: Deconvoluted ^{29}Si (left) (B_0 = 14.1 T, v_R = 10 kHz) and ^{27}Al (right) MAS NMR spectra (B_0 = 14.1 T, v_R = 20 kHz) of the (calcium,alkali)-aluminosilicate gels for samples A - D as marked. Deconvoluted resonances (bottom curve) attributed to sites within the precursor are marked in green, deconvoluted

resonances attributed to newly formed sites in the reaction product are marked in blue, the simulated spectrum is marked in red (middle curve) and the MAS NMR spectrum is marked in black (top curve).

3.2 ^{27}Al MAS and 3QMAS NMR

The ^{27}Al MAS NMR spectra of the (calcium,alkali)-aluminosilicate gel frameworks (Figure 1) alone do not provide sufficient resolution to allow identification of individual chemical sites, beyond general identification of Al coordination environments. The only visibly significant difference between samples is the absence of the intense, sharp octahedral Al resonance at approximately 9 ppm from sample C, while this is observed in all other samples. A detailed discussion and interpretation of ^{27}Al MAS NMR spectra for these samples collected at 12 kHz has been published previously[4, 36], and the spectral features visible here are consistent with those identified in that study.

The broad tetrahedral Al resonance centred at approximately 57 ppm in the spectra of the precursors is due to a distribution of Al environments within the X-ray amorphous phase in the precursor, as identified by XRD[6, 10] (Figure S1, Supporting Information). The low intensity resonance centred at approximately 9 ppm in the spectra of the precursors (Figure S2, Supporting Information) is attributed to octahedral Al within a similar environment to that found in the glassy phase of GGBFS[10].

The low intensity broad resonance centred at approximately 58 ppm in the spectra of the (calcium,alkali)-aluminosilicate gels is assigned to Al in a significantly distorted tetrahedral environment in C-(A)-S-H exhibiting low crystallinity and amorphous N-A-S-H[36]. The high intensity narrow resonance at approximately 9 ppm in the (calcium,alkali)-aluminosilicate gel spectra is due to Al in a well-defined octahedral coordination within AFm-type layered double hydroxide reaction products[4].

Due to the significant overlap of resonances and multiple broadening mechanisms, it is not possible to accurately deconvolute and simulate the ^{27}Al MAS spectra without additional information. Consequently, ^{27}Al 3QMAS spectra were obtained to enable separation of these overlapping resonances.

The iso-sheared ^{27}Al 3QMAS spectra for the calcium aluminosilicate gel reaction products, along with projections along the δ_{1Q} and δ_{3Q} axes, are presented in Figure 2 (those for the calcium aluminosilicate precursors are presented in Figure S1, Supporting Information). A broad distribution of resonances in the Al^{IV}, region of the spectra (centred at approximately (60 ppm, 68 ppm) in the (δ_{3Q}, δ_{1Q}) dimensions) is observed for all precursors. This is assigned to Al(OSi)$_4$ species within the highly polymerised

amorphous aluminosilicate phase present in the precursors which are likely to exhibit significant variations in bond lengths and angles[36, 44], consistent with the observed distributions of both chemical shifts and quadrupolar parameters. These species are charge balanced by Ca^{2+} from the depolymerised calcium silicate phase in the precursors[36].

Alkali-activation of all precursors results in a broad resonance in the ^{27}Al 3QMAS spectra centred at approximately (61 ppm, 65 ppm) in the (δ_{3Q}, δ_{1Q}) dimensions, attributed to tetrahedral Al linked to tetrahedral Si via oxygen bridges (i.e. Si^{IV}-O-Al^{IV}) within the disordered aluminosilicate chains of the C-A-S-H gel identified by XRD[10, 12-13], as well as $Al(OSi)_4$ species from remnant precursor particles. A narrow resonance at approximately (9.5 ppm, 11 ppm) in the (δ_{3Q}, δ_{1Q}) dimensions in the 3QMAS spectra for gels A, B and D is assigned to octahedral Al within AFm-type layered double hydroxide reaction products[4, 13, 29, 45].
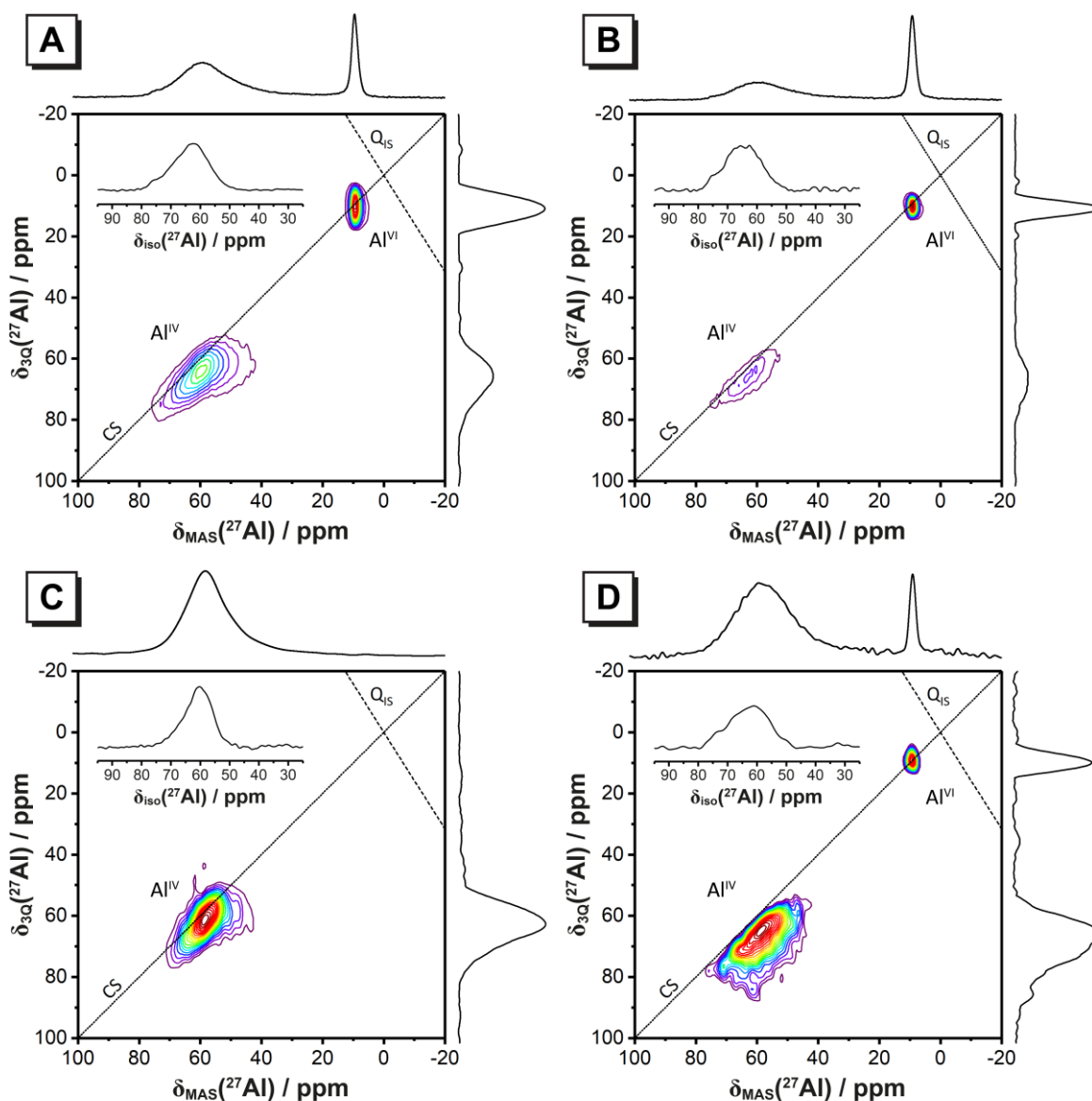
Figure 2: ^{27}Al MAS and 3QMAS NMR spectra (B_0 = 14.1 T, ν_R = 20 kHz) of the (calcium,alkali)-aluminosilicate reaction product for samples A-D as marked. Spectra are sheared using traditional single axial iso-shearing in the δ_{3Q}, δ_{1Q} axes by a factor of 19/12, 0, respectively, to give an isotropic component in the δ_{3Q} (F1) dimension and an anisotropic component in the δ_{1Q} (F2) dimension. The isotropic (δ_{3Q}) projection is shown on the vertical axis and the single pulse MAS NMR spectra are shown on the horizontal axis for comparison. The chemical shift (CS) and quadrupolar induced shift (Q_{IS}) axes are indicated by dotted and dashed lines, respectively. The inset in each 3QMAS spectra shows ^{27}Al isotropic slices (taken through the centre of gravity of each Al^{IV} resonance) extracted from the biaxial Q-sheared ^{27}Al 3QMAS NMR spectra for each sample (see Figure S4, Supporting Information).

Biaxial Q-shearing was used to achieve orthogonal separation of chemical shielding and quadrupolar broadening mechanisms in the [27]Al 3QMAS spectra for these samples (Figure S4, Supporting Information). [27]Al isotropic slices taken through the centre of gravity of each Al[IV] resonance and extracted from the biaxial-Q sheared [27]Al 3QMAS spectra (inset of each plot in Figure 2) show an asymmetrical distribution of Al[IV] chemical shifts, suggesting contributions from multiple Al[IV] sites.

Simulations of the [27]Al MAS spectra, with associated deconvolutions, are presented in Figure 1 and Figure S1, Supporting Information. The relative intensity, δ_{iso} and C_Q for each identified Al environment within the precursor and alkali-activated samples, as well as the mean Al-O-Si bond angle (α) for each Al[IV] environment (which can be calculated from the mean δ_{iso} using equation 2[46]), were obtained by simulation of the [27]Al MAS spectra and are given in Table 2 and 3. Simulations of anisotropic slices for each resonance identified in the [27]Al 3QMAS spectra were used to obtain the δ_{iso} and C_Q of each resonance observed in the 3QMAS spectra. These parameters were then used as starting points to guide simulation of the [27]Al MAS spectra, with the δ_{iso} and C_Q of each resonance in the [27]Al MAS spectra being adjusted as necessary (to account for spectral differences which arise because of differences in phasing one-dimensional and two-dimensional spectra) to fit of the data. It should be noted that as these samples exhibit extensive disorder, the δ_{iso} and C_Q values provided in Table 2 and 3 indicate the average of a distribution of these parameters for each site.

$$\alpha = \frac{137 - \delta_{iso}}{0.532} \tag{2}$$

Table 2: [27]Al parameters extracted from the 3QMAS spectra of the calcium aluminosilicate precursors for each sample as marked.

Sample	Site	Relative integral area (%)	δ_1 (ppm)	δ_2 (ppm)	δ_{iso} (ppm)	$\delta_{iso\ fit}$ (ppm)	C_Q (MHz)	Assignment	Si[IV]-O-Al[IV] bond angle[‡]
	Al[IV]$_1$	77	68.9	61.0	66.0	74.47	5.02	Si[IV]-O-Al[IV]	117.5
	Al[IV]$_2$	21	66.5	58.4	63.5	63.85	6.76	Ca^{2+} balanced Si[IV]-O-Al[IV]	137.5
Precursor A	Al[VI]$_1$	-	-	-	-	-	-	Charge balancing Al[VI]	-
	Al[VI]$_2$	2	-	-	-	13.89	5.43	Al[VI]	-
Precursor B	Al[IV]$_1$	76	78.1	70.0	75.1	75.25	2.47	Si[IV]-O-Al[IV]	116.1
	Al[IV]$_2$	20	67.6	58.9	64.3	65.63	6.43	Ca^{2+} balanced Si[IV]-O-Al[IV]	134.2

Sample	Site	Relative integral area (%)	δ_1 (ppm)	δ_2 (ppm)	δ_{iso} (ppm)	$\delta_{iso\,fit}$ (ppm)	C_Q (MHz)	Assignment	Si^{IV}-O-Al^{IV} bond angle
	Al^{VI}_1	-	-	-	-	-	-	Charge balancing Al^{VI}	-
	Al^{VI}_2	4	-	-	-	12.91	5.60	Al^{VI}	-
Precursor C	Al^{IV}_1	6	70.3	62.9	67.6	74.94	3.37	Si^{IV}-O-Al^{IV}	116.7
	Al^{IV}_2	94	61.0	52.8	58.0	62.61	5.34	Ca^{2+} balanced Si^{IV}-O-Al^{IV}	139.8
	Al^{V}_1	-	-	-	-	-	-	Charge balancing Al^{V}	-
Precursor D	Al^{IV}_1	15	70.1	62.4	67.2	74.79	4.02	Si^{IV}-O-Al^{IV}	116.9
	Al^{IV}_2	85	65.6	57.5	62.6	63.04	4.97	Ca^{2+} balanced Si^{IV}-O-Al^{IV}	139.0
	Al^{VI}_1	-	-	-	-	-	-	Charge balancing Al^{VI}	-

δ_1 and δ_2 are the centre of gravity of the resonance in the isotropic (δ_{3Q}) and anisotropic (δ_{1Q}) dimensions, respectively, δ_{iso} is the isotropic chemical shift determined from Eq.1, and $\delta_{iso\,fit}$ and C_Q are the isotropic chemical shift and quadrupolar coupling constant, respectively, obtained by simulating the anisotropic cross sections and 1D ^{27}Al MAS spectra with the asymmetry parameter (η) assumed to be equal to zero.

‡ Equation 2 is only valid for tetrahedrally coordinated Al.

Table 3: ^{27}Al parameters extracted from the 3QMAS spectra of the (calcium,alkali)-aluminosilicate gels for each sample as marked.

Sample	Site	Relative integral area (%)[†]	δ_1 (ppm)	δ_2 (ppm)	δ_{iso} (ppm)	$\delta_{iso\,fit}$ (ppm)	C_Q (MHz)	Assignment	Si^{IV}-O-Al^{IV} bond angle[‡]
	Al^{IV}_1	1	77.4	73.0	75.8	73.0	1.00	q^2(P) Al^{IV}	120.3
	Al^{IV}_2	20	72.9	68.3	71.2	66.0	2.00	q^2(B) Al^{IV}	133.5
	Al^{IV}_3	39	67.2	61.0	64.9	60.0	4.10	q^3 Al^{IV} in C-A-S-H and q^4 Al^{IV} in N-A-S-H	144.7
Gel A	Al^{V}_1	20	63.7	47.0	57.5	48.0	7.00	Charge balancing Al^{V} in C-A-S-H interlayers	-
	Al^{VI}_1	6	6.0	13.0	8.6	11.85	2.08	C_4AH_{13}	-
	Al^{VI}_2	1	9.5	9.5	9.5	9.56	1.51	Hc/Mc	-
Gel B	Al^{IV}_1	1	76.8	73.3	75.5	73.0	1.00	q^2(P) Al^{IV}	120.3
	Al^{IV}_2	17	70.6	65.6	68.7	66.0	2.00	q^2(B) Al^{IV}	133.5

Gel	Site	I†	δ_1	δ_2	δ_{iso}	$\delta_{iso\,fit}$	C_Q	Assignment	‡
	Al^{IV}_3	28	65.5	60.3	63.6	60.0	4.10	q^3 Al^{IV} in C-A-S-H and q^4 Al^{IV} in N-A-S-H	144.7
	Al^{V}_1	12	-	-	-	48.0	7.00	Charge balancing Al^{V} in C-A-S-H interlayers	-
	Al^{VI}_1	9	-	-	-	11.85	2.08	C_4AH_{13}	-
	Al^{VI}_2	29	9.5	9.3	9.4	9.25	1.51	Hc/Mc	-
	Al^{VI}_3	4	-	-	-	4.50	2.00	TAH	-
Gel C	Al^{IV}_1	1	71.4	64.0	68.7	73.0	1.00	q^2(P) Al^{IV}	120.3
	Al^{IV}_2	17	64.6	58.3	62.3	66.0	2.00	q^2(B) Al^{IV}	133.5
	Al^{IV}_3	72	62.5	48.2	57.2	60.0	4.10	q^3 Al^{IV} in C-A-S-H and q^4 Al^{IV} in N-A-S-H	144.7
	Al^{V}_1	10	-	-		48.0	7.00	Charge balancing Al^{V} in C-A-S-H interlayers	-
Gel D	Al^{IV}_1	1	77.1	71.3	75.0	73.0	1.00	q^2(P) Al^{IV}	120.3
	Al^{IV}_2	22	71.6	65.4	69.3	66.0	2.00	q^2(B) Al^{IV}	133.5
	Al^{IV}_3	49	65.7	59.0	63.2	60.0	4.10	q^3 Al^{IV} in C-A-S-H and q^4 Al^{IV} in N-A-S-H	144.7
	Al^{V}_1	8	-	-	-	48.0	7.00	Charge balancing Al^{V} in C-A-S-H interlayers	-
	Al^{VI}_1	4	-	-	-	11.85	2.08	C_4AH_{13}	-
	Al^{VI}_2	13	9.7	9.3	9.6	9.18	1.22	Hc/Mc	-
	Al^{VI}_3	3	-	-	-	4.50	2.00	TAH	-

δ_1 and δ_2 are the centre of gravity of the resonance in the isotropic (δ_{3Q}) and anisotropic (δ_{1Q}) dimensions, respectively, δ_{iso} is the isotropic chemical shift determined from Eq.1, and $\delta_{iso\,fit}$ and C_Q are the isotropic chemical shift and quadrupolar coupling constant, respectively, obtained by simulating the anisotropic cross sections and 1D ^{27}Al MAS spectra with the asymmetry parameter (η) assumed to be equal to zero.

† The relative integrated intensity for each site in the spectra for the (calcium,alkali)-aluminosilicate gels is normalised as a proportion of the sum of the sites within the reaction product. Precursor component contributions were observed for all (calcium,alkali)-aluminosilicate gel spectra and are shown in Figure 1.

‡ Equation 2 is only valid for tetrahedrally coordinated Al.

The resonance attributed to Al(OSi)$_4$ species charge balanced by Ca^{2+} or AlO$_4^-$ in the depolymerised calcium silicate phase in the precursors exhibits similar δ_{iso} and C_Q values to those of disordered q^3 and q^4 Al sites within GGBFS[16], consistent with previous observations of Al site similarity between these precursors and the aluminosilicate glass in GGBFS[4, 36] and substantiating the site assignments made here.

Three distinct Al^{IV} environments attributed to Al in bridging tetrahedra (q^2(B)), Al in crosslinking tetrahedra (q^3) and, tentatively, to Al in paired tetrahedra (q^2(P)), within the C-A-S-H gel (see Figure 3) are identified in the deconvoluted ^{27}Al MAS NMR spectra of each (calcium,alkali)-aluminosilicate gel[5, 29, 47-48]. The low C_Q values of the q^2(P) (pairing) Al species are half that of the q^2(B) (bridging) Al species, indicating a high degree of EFG symmetry for the q^2(P) (pairing) Al species which suggest that this species is closely linked to lower valence charge balancing species (i.e. H$^+$ or Na$^+$)[49-50], and less EFG symmetry for the q^2(B) (bridging) Al species which suggests this species is closely linked with higher valence charge balancing species (i.e. Ca^{2+})[49-50]. The presence of multiple Al^{IV} resonances in the spectra for each gel is confirmed by the asymmetric distribution of isotropic chemical shifts in the ^{27}Al isotropic slices extracted from the biaxial Q-sheared ^{27}Al 3QMAS spectra (Figure S3, Supporting Information). In particular, the presence of the resonance at δ_{iso} = 73.0 ppm (attributed tentatively to q^2(P) sites) is observed unambiguously.

The explicit observation of q^2(P) sites contrasts with the standard interpretation of C-A-S-H, which excludes Al from substituting for Si into pairing tetrahedra[42, 51]. Substitution of Al into paired tetrahedra within C-A-S-H aluminosilicate chains has been thought to be strongly disfavoured[51], and there is a strong thermodynamic preference of Al substitution into bridging tetrahedra within the C-A-S-H gel[52] and tobermorite[47]. Molecular dynamics atomistic simulations of Al in C-S-H gels, however, have shown Al substitution into these sites is possible in C-A-S-H systems, and will only reach significant concentration at high bulk Al concentrations[53]. It has also been suggested that the existence of Al within these sites may explain the limitations in the ability of the current structural models to fully describe the bulk composition of alkali-activated slag binders[42].

Deconvolution of ^{29}Si MAS NMR spectra for the (calcium,alkali)-aluminosilicate gels includes site assignments consistent with the standard interpretation of C-A-S-H[42, 51] (Figure 1), however a reaction product site tentatively assigned to Q^0 species could not be clearly explained[4]. These sites have also been identified in alkali-activated slags in the past, and either left unassigned to a specific chemical environment[42], attributed to partially hydrated silicate monomers[5-6, 45] or, less commonly, attributed to Q^0 components of anhydrous slag that have not reacted congruently[5]. Sites resonating in this region of ^{29}Si MAS NMR spectra of alkali-activated slag have also been attributed to Q^1(1Al) species[12], or to

numerous Q^1 species without further specification of the chemical environments[6, 10]. ^{1}H-^{29}Si cross polarisation (CP) MAS NMR data provides preferential enhancement of the intensity of Si sites in close proximity to protons, i.e. those in hydrated reaction products within these (calcium,alkali) aluminosilicate gels. For the (calcium,alkali) aluminosilicate gels examined in this study, ^{1}H-^{29}Si CP MAS NMR data published previously showed significant intensity in the region tentatively attributed to Q^0 sites (-76 ppm), indicating that these sites are at least partially hydrated. The inability to clearly define this species in alkali-activated slags or C-A-S-H gels in the past suggests an improved description of these sites is needed.

The presence of Q^1(1Al) species necessitates the presence of q^2(P) sites because tetrahedral site vacancies only occur in the bridging position of C-A-S-H gel aluminosilicate chains[5, 42]. The presence of Q^2(2Al) and Q^3(2Al) sites also necessitate the presence of q^2(P) sites due to the structural constraints of the Cross-linked Substituted Tobermorite Model (CSTM) description of C-A-S-H (see Figure 3)[42], however these sites resonate in the same region as Q^1 and Q^2 sites. Due to the exclusion of Al from substituting for Si into pairing tetrahedra in the standard interpretation of C-A-S-H[42, 51], ^{29}Si MAS NMR resonances within these regions are often attributed solely to Q^1 and Q^2 sites. Due to the previous observation of ^{29}Si MAS NMR resonances within Q^0/Q^1(1Al), Q^1/Q^2(2Al) and Q^2/Q^3(2Al) regions of the spectra for the (calcium,alkali)-aluminosilicate gels examined here[4], and the inability to clearly attribute the Q^0 site to a specific chemical environment, the presence of Q^1(1Al), Q^2(2Al) and Q^3(2Al) species is consistent with the data. This, in conjunction with the ^{27}Al MAS and 3QMAS observations discussed above, substantiate the tentative identification of q^2(P) sites here.

The inability to clearly assign ^{29}Si MAS NMR resonances of alkali-activated slag in the Q^0/Q^1(1Al) region to a particular chemical environment in the past[5-6, 42, 45], as well as the observation of numerous Q^1 sites[6, 10] may be explained by the presence of Q^1(1Al) species, and consequently q^2(P) species, in the samples investigated. This is substantiated by significant intensity in the Q^1/Q^2(2Al) and Q^2/Q^3(2Al) regions of the ^{29}Si MAS NMR spectra in these studies[5-6, 10, 42, 45].

Previously published ^{27}Al MAS and 3QMAS NMR studies have observed two distinct q^2 sites within alkali-activated slag binders[5-6, 54-55], synthetic C-A-S-H gels[48] and tobermorite[47] and have speculated the possibility of Al substitution into these paired tetrahedra in (calcium,alkali)-aluminosilicate gel systems with Ca/(Al+Si) > 0.95 [5, 48]. The explicit observation of q^2(P) sites in the ^{27}Al MAS and 3QMAS NMR data of all samples presented here suggests that the bulk Ca/(Al+Si) does not need to be significantly high for this substitution to occur, and the resonance attributed to these sites is more pronounced in samples with higher bulk Al content (samples A and B). The relative amount of q^2(P) sites is small, however, with q^2(P) sites accounting for 0.7-1.5% of all Al sites in the (calcium,alkali)-

aluminosilicate gels and 1.2-2.2% of all Al^{IV} sites in the (calcium,alkali)-aluminosilicate gels. The bulk of Al^{IV} substitution occurs within q^3 and q^2(B) sites, with approximately twice the Al^{IV} substitution occurring in q^3 sites compared to q^2(B) sites, consistent with the preference of Al to be located in crosslinked and polymerised sites[5, 8, 42].
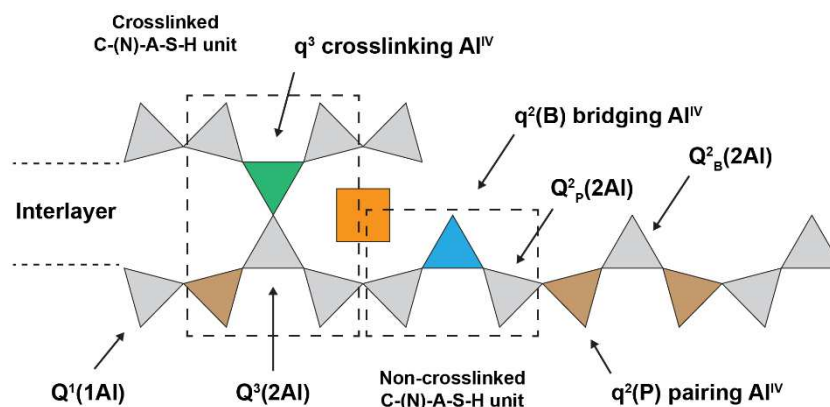
Figure 3: Schematic representation of Al sites within C-A-S-H type gels showing crosslinking q^3 Al tetrahedra (green triangle), bridging q^2(B) Al tetrahedra (blue triangle), pairing q^2(P) Al tetrahedra (brown triangle) and charge balancing Al^V (orange square). Si tetrahedra are shown by the grey triangles, and charge balancing alkali cations and protons are omitted for clarity. Adapted with permission from ref. 42. Copyright (2013) American Chemical Society.

C_Q values for the q^3 (crosslinking) species (4.0 MHz) indicate significant perturbation of the EFG and a high degree of structural asymmetry, consistent with the large distribution of δ_{iso} values and disorder observed for these environments within the C-A-S-H gel. Si^{IV}-O-Al^{IV} sites charge balanced by Na^+ within the N-A-S-H gel observed in these samples previously by ^{29}Si, ^{27}Al and ^{23}Na MAS NMR are also expected to resonate at $\delta_{iso} \approx 61$ ppm and will contribute in this region of each (calcium,alkali)-aluminosilicate gel [27]Al MAS and 3QMAS spectrum[31].

The relative proportions of Al in q^3 and q^4 environments within each (calcium,alkali)-aluminosilicate gel increase with increasing bulk Al content (Table 4), consistent with the known structural preference for Al to be located in crosslinking sites[5, 42]. Consequently, increased Al content results in increased formation of highly polymerised crosslinking environments[4] until the bridging sites are saturated with Al[56]. The proportion of q^3 crosslinking to q^2 non-crosslinking sites is consistent with the deconvolutions of ^{29}Si MAS NMR data for these (calcium,alkali)-aluminosilicate gels[4] (Figure 1) and with the CSTM structural description of C-A-S-H[42].

Table 4: Relative proportion of Al^{IV} sites in C-A-S-H and N-A-S-H (%)

Sample	q^2(P) in C-A-S-H	q^2(B) in C-A-S-H	q^3 in C-A-S-H + q^4 in N-A-S-H
A	1.2	33.0	65.8
B	2.2	36.5	61.3
C	1.6	22.6	75.8
D	1.1	33.9	65.0

A single, asymmetrical (C$_Q$ = 7.0 MHz) Al^V environment exhibiting a consistent lineshape across all samples is identified in each (calcium,alkali)-aluminosilicate gel, and is attributed to charge balancing Al^V within C-A-S-H gel interlayers[5]. The existence of five-coordinated Al within the C-A-S-H gel interlayer has been hypothesised in the literature[57-59] however this species is not included in current structural descriptions of C-A-S-H gels[42]. The relative amount of this Al^V environment within the C-A-S-H gel increases with increasing Al content. It is likely that this is due to structural limitations on the amount of Al substitution into tetrahedral sites within the aluminosilicate chains of the C-A-S-H gel[42], with increased Al content beyond this limitation resulting in increased charge balancing Al^V species.

Al^{VI} environments attributed to Al in hemicarbonate AFm (Hc), monocarbonate AFm (Mc) and hydroxy-AFm (C$_4$AH$_{13}$) layered double hydroxide reaction products are identified in the (calcium,alkali)-aluminosilicate gel for each sample[4, 13, 29, 45]. A resonance attributed to the 'third aluminate hydrate', an amorphous nanoscale aluminate hydrate phase precipitated at the surface of the C-S-H type gels[4, 45, 58, 60] which has also been noted in alkali-activated slags[10, 13, 61], is resolved in the deconvoluted ^{27}Al MAS NMR spectra for (calcium,alkali)-aluminosilicate gel samples B and D. This is consistent with stoichiometric arguments and thermodynamic modelling which suggest that the presence of TAH is likely to be linked to high concentrations of available Ca and Al[2, 11, 62].

Mean Si^{IV}-O-Al^{IV} bond angles for each species (q^2(P), q^2(B) and q^3) are identical across all (calcium,alkali)-aluminosilicate gel samples (120.3º, 133.5º, 144.7º, respectively) suggesting strong structural similarity between the C-A-S-H gels formed in each case despite differing initial precursor composition. These bond angles are consistent with the geometry of clinotobermorite-based structural models for (calcium,alkali)-aluminosilicate gel frameworks[63].

3.3 ^{17}O MAS and 3QMAS NMR

The ^{17}O MAS NMR spectrum for each (calcium,alkali)-aluminosilicate gel (Figure 4) shows a broad large intensity resonance centred at approximately 110 ppm, as well as a low intensity broad resonance centred at approximately 50 ppm. These resonances are assigned respectively to non-bridging oxygen (NBO) species associated with Ca within the C-A-S-H gel, and to bridging oxygen (BO) within both crosslinked and non-crosslinked aluminosilicate chains in C-A-S-H and aluminosilicate frameworks in present in the N-A-S-H gel, in each (calcium,alkali)-aluminosilicate gel[16-17, 25, 31].

Each ^{17}O MAS NMR spectrum exhibits extensive line broadening. The resonances centred at 110 ppm extend across a region in which non-bridging oxygen (NBO) species associated with varying numbers of Ca atoms have been observed[17, 24-25], while the resonance centred at 50 ppm extends across a region in which Si^{IV}-O-Si^{IV}, Si^{IV}-O-Al^{IV} and Al^{IV}-O-Al^{IV} linkages have been observed[17, 64-65]. ^{17}O 3QMAS spectra were obtained to separate these overlapping resonances.

Iso-sheared ^{17}O 3QMAS spectra, along with projections along the δ_{1Q} and δ_{3Q} axes, for (calcium,alkali)-aluminosilicate gel samples A, B and D are also presented in Figure 4. Biaxial shearing of each ^{17}O 3QMAS spectra does not resolve any additional resonances. It was not possible to obtain a suitable ^{17}O 3QMAS spectrum for (calcium,alkali)-aluminosilicate gel C due to the very low signal/noise ratio attained for this mix, low efficiency of the 3QMAS pulse sequence and/or low degree of isotopic enrichment.
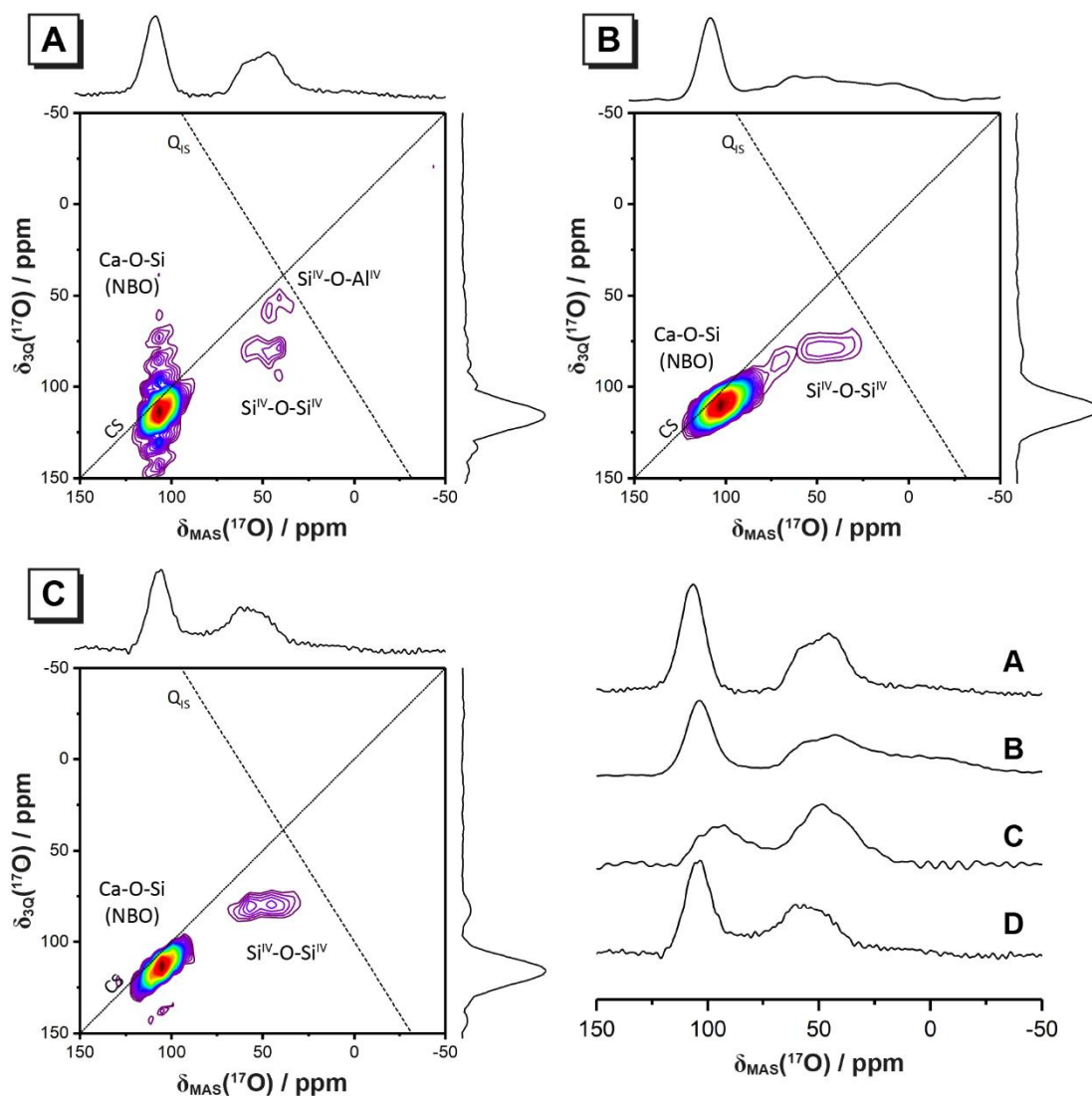
Figure 4: ^{17}O MAS and 3QMAS NMR spectra (B_0 = 14.1 T, v_R = 20 kHz) of the (calcium,alkali)-aluminosilicate gels for samples A - D as marked. ^{17}O 3QMAS NMR spectra are sheared using traditional single axial iso-shearing in the δ_{3Q}, δ_{1Q} axes by a factor of 19/12, 0, respectively, to give an isotropic component in the δ_{3Q} (F1) dimension and an anisotropic component in the δ_{3Q} (F2) dimension. The isotropic (δ_{3Q}) projection is shown on the vertical axis and the single pulse MAS NMR spectra are shown on the horizontal axis for comparison. The chemical shift (CS) and quadrupolar induced shift (Q_{IS}) axes are indicated by dotted and dashed lines, respectively. It was not possible to obtain a suitable ^{17}O 3QMAS spectrum for (calcium,alkali)-aluminosilicate gel C due to the very low signal/noise ratio attained for this mix, low efficiency of the 3QMAS pulse sequence and/or low degree of isotopic enrichment.

Two distinct resonances are resolved in the iso-sheared [17]O 3QMAS spectra for each (calcium,alkali)-aluminosilicate gel. A high intensity broad resonance centred at approximately (114 ppm, 106 ppm) in the (δ_{3Q}, δ_{1Q}) dimensions attributed to non-bridging oxygen associated with Ca atoms is observed in all spectra[24]. This resonance is primarily broadened along the CS axis in all spectra indicating a large distribution in δ_{iso} with a much narrower distribution in quadrupolar parameters. A resonance with much lower intensity is also observed, centred at approximately (79 ppm, 50 ppm) in the (δ_{3Q}, δ_{1Q}) dimensions attributed to bridging oxygen in Si^{IV}-O-Si^{IV} linkages[66]. A third low intensity resonance is also observed in the spectrum for sample A at (55 ppm, 42 ppm) in the (δ_{3Q}, δ_{1Q}) dimensions and is attributed to Si^{IV}-O-Al^{IV} linkages, consistent with the higher Al content in this sample. These low intensity resonances are both broadened equally in the CS and Q_{IS} axes indicating significant distributions of δ_{iso} and quadrupolar parameters. Substitution of Al for Si will result in increased shielding and a reduction in perturbation of the EFG of the bridging oxygen nuclei, and consequently the resonance due to Si^{IV}-O-Si^{IV} sites is expected to exhibit a higher δ_{iso} than that of Si^{IV}-O-Al^{IV} sites[17, 24, 64-65].

Oxygen within Ca-OH in the CaO layers within the C-A-S-H gel (where a proton substitutes for a silicon atom) has been observed previously in C-S-H gels[24]. Si-OH environments in Q^2 and Q^3 silicon environments previously identified in the C-A-S-H gel in these samples by ^{29}Si MAS NMR[4], as well as hydroxyl groups within AFM-type layered double hydroxides phases and molecular water tightly bound within the C-A-S-H gel[24, 67], are also expected to resonate at approximately δ_{iso} = 5 ppm and account for the intensity in this region of the ^{17}O MAS NMR spectra for these samples.

Increased bulk Ca content results in an increase in coordination number around non-bridging oxygen nuclei in Ca-O-Si sites, as well as an increase in the proportion of Ca-OH sites within the CaO layers in the C-A-S-H gel in higher Al samples A and B, indicating a shift towards more Ca-rich C-A-S-H. For samples with high bulk Ca content, increased Al content causes a reduction in resonances attributed to oxygen associated with Ca ions, and an increase in resonances attributed to bridging oxygen sites within the N-A-S-H gel. In these samples increased bulk Al content reduces the proportion of Si^{IV}-O-Si^{IV} and increases the proportion of Si^{IV}-O-Al^{IV} sites. These changes are consistent with previous observations by ^{29}Si MAS NMR[4] and indicate an increase in Al substitution within the C-A-S-H gel, as well as an overall decrease in the amount of C-A-S-H gel present within the samples, and an increase in N-A-S-H.

3.4 ^{23}Na MAS and 3QMAS NMR

The ^{23}Na MAS NMR spectrum (Figure 5) for each (calcium,alkali)-aluminosilicate gel exhibits broad resonance with a maximum at δ_{obs} = -5 ppm, attributed to Na^+ cations associated with aluminium-centred tetrahedra in a charge balancing role, in both C-(N)-A-S-H[13, 68] and N-A-S-H gel frameworks[69-70]. This resonance is observed in the spectrum of each (calcium,alkali)-aluminosilicate gel at all ages, indicating no obvious observable variation in the environments of the charge-balancing Na^+ cations in these binders. A small shoulder at δ_{obs} = -18 ppm is observed in the ^{23}Na MAS NMR spectra of all samples, and is much more pronounced in samples C and D. The position and broad nature of this resonance suggests the presence of Na experiencing much greater electron density than that at δ_{obs} = -5 ppm, within a very disordered phase, or which has sorbed to the surfaces of the nanostructured gel[4]. ^{23}Na MAS NMR spectra of the precursors (Figure S2, Supporting Information) suggest that this resonance is at least partly due to remnant precursor particles within the (calcium,alkali)-aluminosilicate gel.

Iso-sheared ^{23}Na 3QMAS spectra for each (calcium,alkali)-aluminosilicate gel, along with projections along the δ_{1Q} and δ_{3Q} axes are presented in Figure 5. A moderately broad resonance centred at (2.8 ppm, -3.4 ppm) in the (δ_{3Q}, δ_{1Q}) axes is observed in the spectra for the (calcium,alkali)-aluminosilicate gel for samples A and B. Broadening of this resonance occurs to similar extents along the CS and Q_{IS} axes.

A much narrower resonance centred at approximately (-8.5ppm, -4.0 ppm) in the (δ_{3Q}, δ_{1Q}) axes is observed in the spectra for the (calcium,alkali)-aluminosilicate gel samples C and D. Broadening of this resonance occurs to similar extents along the CS and Q_{IS} axes in sample C, however in sample D broadening occurs primarily along the CS axis, indicating a much narrower distribution of quadrupolar parameters for this sample. This is likely to be due to greatly reduced N-A-S-H gel content and increased ordering of the C-(N)-A-S-H gel in sample D compared with sample C[4]. The shift of this resonance along the Q_{IS} axis toward higher frequencies suggests that it is linked to ionic species which induce larger perturbations in the EFG surrounding the Na nucleus, consistent with closer association with Al^{3+} in the C-(N)-A-S-H gel interlayer.

The broader resonance located at approximately (2.8 ppm, -3.4 ppm) in the (δ_{3Q}, δ_{1Q}) dimensions, respectively, is attributed to Na^+ cations associated with aluminium-centred tetrahedra in a charge balancing role within both C-(N)-A-S-H[13, 68] and N-A-S-H gel frameworks[69-70]. This resonance is observed to shift toward lower frequency (more negative chemical shifts) with reduced bulk Al content and increasing bulk Ca content (sample D), consistent with increased shielding of the Na nuclei due to increased association with C-(N)-A-S-H in a charge balancing capacity, and a relative reduction in the

amount of N-A-S-H gel present within the samples[4]. It is expected that charge balancing Na^+ species in C-(N)-A-S-H and N-A-S-H gels will exhibit distinct resonances, and it is likely that the shift of the resonance at (2.8 ppm, -3.4 ppm) in the (δ_{3Q}, δ_{1Q}) dimensions is due to the presence of different proportions of each of these sites. Due to closer association ionic species with larger charge as well as increased shielding of Na within C-(N)-A-S-H compared to N-A-S-H, Na within C-(N)-A-S-H is likely to exhibit lower δ_{iso} and greater C_q values than Na within N-A-S-H[28, 31, 49-50]. In the samples examined here these sites exhibit very similar resonances which are not able to be individually resolved in the iso-sheared [23]Na 3QMAS or biaxially sheared [23]Na 3QMAS spectra.

The relative intensity, δ_{iso} and C_Q for each identified Na environment within the (calcium,alkali)-aluminosilicate gel (obtained by simulation of the [23]Na MAS spectra) are given in Table 5. Deconvolutions of the [23]Na MAS spectra are provided in Figure 5. Again, it should be noted that as these samples exhibit extensive disorder, the δ_{iso} and C_Q values provided in Table 5 do not indicate a single value but rather indicate the average of a distribution of these parameters for each site.

Two distinct Na environments attributed to Na within remnant precursor particles are identified in the deconvoluted ^{23}Na MAS NMR (Figure 5 and Figure S2, Supporting Information), due to the presence of 1-2 % wt. Na_2O as stabiliser in the colloidal silica precursor used for precursor synthesis[36]. A single newly formed environment due to charge balancing Na^+ in C-(N)-A-S-H and N-A-S-H gels is also observed in the deconvoluted ^{23}Na MAS NMR spectra. There is no clearly observable change in Na speciation with changes in bulk composition, apart from a reduction in the proportion of charge balancing Na^+ relative to precursor Na species when bulk Ca content increases. This can be attributed to the significantly lower relative Na content within these high-Ca samples (C and D) due to their stoichiometric design (Table 1).
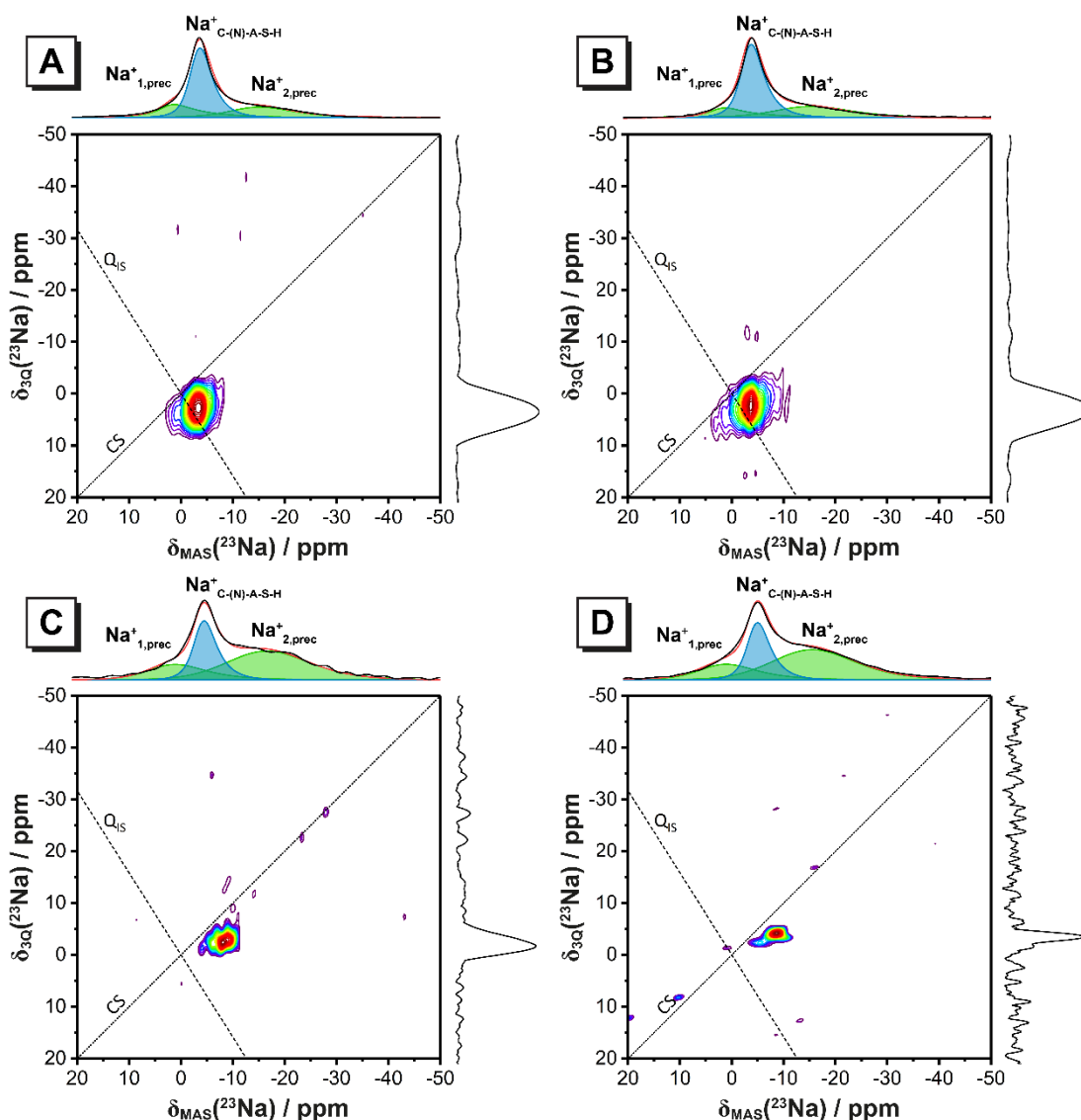
Figure 5: ^{23}Na MAS and 3QMAS NMR spectra (B_0 = 14.1 T, ν_R = 20 kHz) of the (calcium,alkali)-aluminosilicate gels for samples A-D as marked. Spectra are sheared using traditional single axial iso-shearing in the δ_{3Q}, δ_{1Q} axes by a factor of 7/9, 0, respectively, to give an isotropic component in the δ_{3Q} (F1) dimension and an anisotropic component in the δ_{1Q} (F2) dimension. The isotropic (δ_{3Q}) projection is shown on the vertical axis and the single pulse MAS NMR spectra and associated spectral deconvolutions are shown on the horizontal axis for comparison. Deconvoluted resonances are marked in blue, the simulated spectrum is marked in red and the ^{23}Na MAS NMR spectrum is marked in black. The chemical shift (CS) and quadrupolar induced shift (Q_{IS}) axes are indicated by dotted and dashed lines, respectively.

Table 5: [23]Na parameters extracted from the 3QMAS spectra of the (calcium,alkali)-aluminosilicate gels for each aluminosilicate sample as marked.

Sample	Site	Relative integrated area (%)	δ_1 (ppm)	δ_2 (ppm)	δ_{iso} (ppm)	$\delta_{iso\ fit}$ (ppm)	C_Q (MHz)	Assignment
Gel A	Na^+_1	21	3.9	0.9	2.8	1.5	1.6	Precursor Na_2O species
	Na^+_2	56	2.8	-3.3	0.6	-3.7	1.0	Na^+ balancing Si^{IV}-O^--Al^{IV} in N-A-S-H and C-A-S-H
	Na^+_3	23	-	-	-	-13.9	1.6	Precursor Na_2O species
Gel B	Na^+_1	14	4.5	1.5	3.4	1.5	1.6	Precursor Na_2O species
	Na^+_2	59	2.5	-3.6	0.2	-3.8	1.1	Na+ balancing Si^{IV}-O^--Al^{IV} in N-A-S-H and C-A-S-H
	Na^+_3	27	-	-	-	-13.9	1.6	Precursor Na_2O species
Gel C	Na^+_1	20	-2.2	-6.0	3.6	2.0	1.6	Precursor Na_2O species
	Na^+_2	30	-2.3	-8.0	4.4	-4.5	1.1	Na+ balancing Si^{IV}-O^--Al^{IV} in N-A-S-H and C-A-S-H
	Na^+_3	50	-	-	-	-15.0	1.6	Precursor Na_2O species
Gel D	Na^+_1	20	-2.2	-5.4	3.4	2.0	1.6	Precursor Na_2O species
	Na^+_2	29	-4.0	-8.6	5.7	-5.0	1.1	Na+ balancing Si^{IV}-O^--Al^{IV} in N-A-S-H and C-A-S-H
	Na^+_3	51	-	-	-	-13.9	1.6	Precursor Na_2O species

δ_1 and δ_2 are the centre of gravity of the resonance in the isotropic (δ_{3Q}) and anisotropic (δ_{3Q}) dimensions, respectively, δ_{iso} is the isotropic chemical shift determined by Equation 1, d_{Na-O} is the average Na-O interatomic distance determined using Equation 3 and $\delta_{iso\ fit}$, C_Q and η are the isotropic chemical shift, quadrupolar coupling constant and asymmetry parameter, respectively, obtained by simulating the anisotropic cross sections and 1D [23]Na MAS spectra with the asymmetry parameter (η) assumed to be equal to zero.

4. Conclusions

The key structural motifs which assemble to form the C-(N)-A-S-H, C-A-S-H and N-A-S-H gel frameworks are identified through application of ^{17}O, ^{23}Na and ^{27}Al 3QMAS NMR spectroscopy to multiphase ^{17}O-enriched gels. The main reaction product in all samples was a mixed crosslinked/non-crosslinked tobermorite-like C-(N)-A-S-H gel containing varying levels of Al and Na, while additional reaction products were N-A-S-H, monocarbonate AFm, hemicarbonate AFm, hydroxy-AFm (C_4AH_{13}) and the 'third aluminate hydrate'. Al^{IV} within the C-(N)-A-S-H gel substitutes for bridging Si^{IV} primarily in q^3 crosslinking and $q^2(B)$ bridging sites, but is also observed in smaller quantities in $q^2(P)$ pairing sites. Both Al^V species and Na^+ cations are found in the gel interlayer, charge-balancing the AlO_4^- tetrahedra. Na^+ cations are also found sorbed to the gel surface.

Increased bulk Ca content within the reaction mixture promotes the formation of low-Al, high-Ca containing C-(N)-A-S-H exhibiting greater levels of ordering, lower levels of crosslinking sites, increased Ca coordination of non-bridging oxygen atoms and an increase in proton association with CaO layers to form Ca-OH sites. Increased bulk Ca content also promotes the formation of hydroxy-AFm and monocarbonate AFm type phases.

Increased bulk Al content within the reaction mixture promotes an increase in Al substitution within the C-(N)-A-S-H gel overall, an increased proportion of crosslinking sites, and increased gel disorder. Increased bulk Al content also results in increased Al substitution within paired tetrahedra, an increased proportion of charge balancing Al^V species within the gel interlayer and increased formation of the additional disordered N-A-S-H gel with high Al and Na content.

These findings establish new understanding of the molecular interactions which govern the nanostructure of these gels, and how these interactions are controlled by precursor composition and mix formulation. NMR parameters for chemically distinct sites within the C-(N)-A-S-H gel are also identified for the first time. This knowledge is crucial for developing further understanding of the key parameters controlling durability in (calcium,alkali)-aluminosilicate gel, and can in turn be used to develop tailor-made (calcium,alkali)-aluminosilicate gel with specific physical properties for unique applications.

While this study has provided significant advances in our understanding of the nanostructure of these materials, resolving the large number of overlapping resonances in the NMR data of such complex and disordered multi-phase materials remains extremely challenging. Future work applying solid state MAS and MQMAS NMR experiments at high field ($B_0 \geq 14.1$ T) will help overcome these challenges.

Future research focusing on long term phase and structural stability, macroscale engineering properties (e.g. compressive and tensile strength) and nanostructural changes induced by durability phenomena (e.g. carbonation and chloride migration) in these systems will also be vital to further understand these materials which are the basis of modern cements.

5. Supporting Information

Full details of the sample synthesis procedure. Full details of the NMR data processing and fitting procedures. Additional figures (S1-S4) as discussed in the main text.

6. Acknowledgements

References

1.   Provis, J. L.; Bernal, S. A., Geopolymers and Related Alkali-Activated Materials. *Annual Review of Materials Research* **2014**, *44*, 299-327.

2.   Provis, J. L.; van Deventer, J. S. J., *Alkali Activated Materials. State-of-the-Art Report, RILEM TC 224-AAM*; Springer: Dordrecht, 2014; Vol. 13.

3.   Provis, J. L.; Palomo, A.; Shi, C. J., Advances in Understanding Alkali-Activated Materials. *Cement and Concrete Research* **2015**, *78*, 110-125.

4.   Walkley, B.; San Nicolas, R.; Sani, M.-A.; Rees, G. J.; Hanna, J. V.; van Deventer, J. S. J.; Provis, J. L., Phase Evolution of C-(N)-A-S-H/N-A-S-H Gel Blends Investigated Via Alkali-Activation of Synthetic Calcium Aluminosilicate Precursors. *Cement and Concrete Research* **2016**, *89*, 120-135.

5.   Myers, R. J.; Bernal, S. A.; Gehman, J. D.; van Deventer, J. S. J.; Provis, J. L., The Role of Al in Cross-Linking of Alkali-Activated Slag Cements. *Journal of the American Ceramic Society* **2015**, *98*, 996-1004.

6.   Bernal, S. A.; San Nicolas, R.; Myers, R. J.; Mejía de Gutiérrez, R.; Puertas, F.; van Deventer, J. S. J.; Provis, J. L., Mgo Content of Slag Controls Phase Evolution and Structural Changes Induced by Accelerated Carbonation in Alkali-Activated Binders. *Cement and Concrete Research* **2014**, *57*, 33-43.

7.   Walkley, B.; San Nicolas, R.; Sani, M.-A.; Bernal, S. A.; van Deventer, J. S. J.; Provis, J. L., Structural Evolution of Synthetic Alkali-Activated $CaO-MgO-Na_2O-Al_2O_3-SiO_2$ Materials Is Influenced by Mg Content. *Cement and Concrete Research* **2017**, *99*, 155-171.

8.   Myers, R. J.; L'Hôpital, É. M.; Provis, J. L.; Lothenbach, B., Composition-Solubility-Structure Relationships in Calcium (Alkali) Aluminosilicate Hydrate (C-(N,K-)A-S-H). *Dalton Transactions* **2015**, *44*, 13530-44.

9.   Richardson, I. G., The Calcium Silicate Hydrates. *Cement and Concrete Research* **2008**, *38*, 137-158.

10.   Bernal, S. A.; Provis, J. L.; Walkley, B.; San Nicolas, R.; Gehman, J. D.; Brice, D. G.; Kilcullen, A. R.; Duxson, P.; van Deventer, J. S. J., Gel Nanostructure in Alkali-Activated Binders Based on Slag and Fly Ash, and Effects of Accelerated Carbonation. *Cement and Concrete Research* **2013**, *53*, 127-144.

11.   Wang, S.-D.; Scrivener, K. L., ^{29}Si and ^{27}Al NMR Study of Alkali-Activated Slag. *Cement and Concrete Research* **2003**, *33*, 769-774.

12.   Le Saoût, G.; Ben Haha, M.; Winnefeld, F.; Lothenbach, B.; Jantzen, C., Hydration Degree of Alkali-Activated Slags: A ^{29}Si NMR Study. *Journal of the American Ceramic Society* **2011**, *94*, 4541-4547.

13.   Bonk, F.; Schneider, J.; Cincotto, M. A.; Panepucci, H., Characterization by Multinuclear High-Resolution NMR of Hydration Products in Activated Blast-Furnace Slag Pastes. *Journal of the American Ceramic Society* **2003**, *86*, 1712-1719.

14.   Lee, S. K.; Stebbins, J. F., Disorder and the Extent of Polymerization in Calcium Silicate and Aluminosilicate Glasses: O-17 NMR Results and Quantum Chemical Molecular Orbital Calculations. *Geochimica et Cosmochimica Acta* **2006**, *70*, 4275-4286.

15.   Allwardt, J. R.; Lee, S. K.; Stebbins, J. F., Bonding Preferences of Non-Bridging O Atoms: Evidence from ^{17}O MAS and 3QMAS NMR on Calcium Aluminate and Low-Silica Ca-Aluminosilicate Glasses. *American Mineralogist* **2003**, *88*, 949-954.

16.   Shimoda, K.; Tobu, Y.; Kanehashi, K.; Nemoto, T.; Saito, K., Total Understanding of the Local Structures of an Amorphous Slag: Perspective from Multi-Nuclear ([29]Si, [27]Al, [17]O, [25]Mg, and [43]Ca) Solid-State NMR. *Journal of Non-Crystalline Solids* **2008**, *354*, 1036-1043.

17.   Kelsey, K. E.; Allwardt, J. R.; Stebbins, J. F., Ca–Mg Mixing in Aluminosilicate Glasses: An Investigation Using [17]O Mas and 3QMAS and ^{27}Al MAS NMR. *Journal of Non-Crystalline Solids* **2008**, *354*, 4644-4653.

18.   Benoit, M.; Profeta, M.; Mauri, F.; Pickard, C. J.; Tuckerman, M. E., First-Principles Calculation of the 17O NMR Parameters of a Calcium Aluminosilicate Glass. *The Journal of Physical Chemistry B* **2005**, *109*, 6052-6060.

19.	Neuhoff, P. S.; Zhao, P.; Stebbins, J. F., Effect of Extraframework Species on ^{17}O NMR Chemical Shifts in Zeolite A. *Microporous and Mesoporous Materials* **2002**, *55*, 239-251.

20.	Dirken, P. J.; Kohn, S. C.; Smith, M. E.; van Eck, E. R. H., Complete Resolution of Si-O-Si and Si-O-Al Fragments in an Aluminosilicate Glass by ^{17}O Multiple Quantum Magic Angle Spinning NMR Spectroscopy. *Chemical Physics Letters* **1997**, *266*, 568-574.

21.	Pingel, U. T.; Amoureux, J. P.; Anupold, T.; Bauer, F.; Ernst, H.; Fernandez, C.; Freude, D.; Samoson, A., High-Field ^{17}O Nmr Studies of the SiOAl Bond in Solids. *Chemical Physics Letters* **1998**, *294*, 345-350.

22.	Gehman, J. D.; Provis, J. L., Generalized Biaxial Shearing of MQMAS NMR Spectra. *Journal of Magnetic Resonance* **2009**, *200*, 167-172.

23.	Duxson, P. The Structure and Thermal Evolution of Metakaolin Geopolymers. The University of Melbourne, Melbourne, Australia, 2006.

24.	Cong, X.; Kirkpatrick, R. J., ^{17}O MAS NMR Investigation of the Structure of Calcium Silicate Hydrate Gel. *Journal of the American Ceramic Society* **1996**, *79*, 1585-1592.

25.	Cong, X.; Kirkpatrick, R. J., ^{17}O and ^{29}Si MAS NMR Study of B–C_2S Hydration and the Structure of Calcium-Silicate Hydrates. *Cement and Concrete Research* **1993**, *23*, 1065-1077.

26.	Frydman, L.; Harwood, J. S., Isotropic Spectra of Half-Integer Quadrupolar Spins from Bidimensional Magic-Angle-Spinning NMR. *Journal of the American Chemical Society* **1995**, *117*, 5367-5368.

27.	Medek, A.; Harwood, J. S.; Frydman, L., Multiple-Quantum Magic-Angle Spinning NMR: A New Method for the Study of Quadrupolar Nuclei in Solids. *Journal of the American Chemical Society* **1995**, *117*, 12779-12787.

28.	Brus, J.; Kobera, L.; Urbanová, M.; Koloušek, D.; Kotek, J., Insights into the Structural Transformations of Aluminosilicate Inorganic Polymers: A Comprehensive Solid-State NMR Study. *The Journal of Physical Chemistry C* **2012**, *116*, 14627-14637.

29.	Faucon, P.; Charpentier, T.; Bertrandie, D.; Nonat, A.; Virlet, J.; Petit, J. C., Characterization of Calcium Aluminate Hydrates and Related Hydrates of Cement Pastes by ^{27}Al MQ-MAS NMR. *Inorganic Chemistry* **1998**, *37*, 3726-3733.

30.	Rowles, M. R.; Hanna, J. V.; Pike, K. J.; Smith, M. E.; O'Connor, B. H., ^{29}Si, ^{27}Al, ^{1}H and ^{23}Na MAS NMR Study of the Bonding Character in Aluminosilicate Inorganic Polymers. *Applied Magnetic Resonance* **2007**, *32*, 663-689.

31.	Walkley, B.; Rees, G. J.; San Nicolas, R.; van Deventer, J. S. J.; Hanna, J. V.; Provis, J. L., New Structural Model of Hydrous Sodium Aluminosilicate Gels and the Role of Charge-Balancing Extra-Framework Al. *Journal of Physical Chemistry C* **2018**, *122*, 5673-5685.

32.	Sideris, P. J.; Blanc, F.; Gan, Z.; Grey, C. P., Identification of Cation Clustering in Mg–Al Layered Double Hydroxides Using Multinuclear Solid State Nuclear Magnetic Resonance Spectroscopy. *Chemistry of Materials* **2012**, *24*, 2449-2461.

33.	Massiot, D.; Touzo, B.; Trumeau, D.; Coutures, J. P.; Virlet, J.; Florian, P.; Grandinetti, P. J., Two-Dimensional Magic-Angle Spinning Isotropic Reconstruction Sequences for Quadrupolar Nuclei. *Solid State Nuclear Magnetic Resonance* **1996**, *6*, 73-83.

34.	Hung, I.; Trébosc, J.; Hoatson, G. L.; Vold, R. L.; Amoureux, J.-P.; Gan, Z., Q-Shear Transformation for MQMAS and STMAS NMR Spectra. *Journal of Magnetic Resonance* **2009**, *201*, 81-86.

35.	Kobera, L.; Brus, J.; Klein, P.; Dedecek, J.; Urbanova, M., Biaxial Q-Shearing of ^{27}Al 3QMAS NMR Spectra: Insight into the Structural Disorder of Framework Aluminosilicates. *Solid State Nuclear Magnetic Resonance* **2014**, *57–58*, 29-38.

36.	Walkley, B.; San Nicolas, R.; Sani, M.-A.; Gehman, J. D.; van Deventer, J. S. J.; Provis, J. L., Synthesis of Stoichiometrically Controlled Reactive Aluminosilicate and Calcium-Aluminosilicate Powders. *Powder Technology* **2016**, *297*, 17-33.

37.   Walkley, B.; Provis, J. L.; San Nicolas, R.; Sani, M. A.; van Deventer, J. S. J., Stoichiometrically Controlled C–(A)–S–H/N–A–S–H Gel Blends Via Alkali-Activation of Synthetic Precursors. *Advances in Applied Ceramics* **2015**, *114*, 372-377.

38.   Delaglio, F.; Grzesiek, S.; Vuister, G.; Zhu, G.; Pfeifer, J.; Bax, A., NMRPipe: A Multidimensional Spectral Processing System Based on Unix Pipes. *J Biomol NMR* **1995**, *6*, 277-293.

39.   Massiot, D.; Fayon, F.; Capron, M.; King, I.; Le Calvé, S.; Alonso, B.; Durand, J.-O.; Bujoli, B.; Gan, Z.; Hoatson, G., Modelling One- and Two-Dimensional Solid-State NMR Spectra. *Magnetic Resonance in Chemistry* **2002**, *40*, 70-76.

40.   Neuville, D. R.; Cormier, L.; Massiot, D., Al Environment in Tectosilicate and Peraluminous Glasses: A ^{27}Al MQ-MAS NMR, Raman, and Xanes Investigation. *Geochimica et Cosmochimica Acta* **2004**, *68*, 5071-5079.

41.   d'Espinose de Lacaillerie, J.-B.; Fretigny, C.; Massiot, D., Mas Nmr Spectra of Quadrupolar Nuclei in Disordered Solids: The Czjzek Model. *Journal of Magnetic Resonance* **2008**, *192*, 244-251.

42.   Myers, R. J.; Bernal, S. A.; San Nicolas, R.; Provis, J. L., Generalized Structural Description of Calcium-Sodium Aluminosilicate Hydrate Gels: The Cross-Linked Substituted Tobermorite Model. *Langmuir* **2013**, *29*, 5294-306.

43.   Provis, J. L.; Duxson, P.; Lukey, G. C.; van Deventer, J. S. J., Statistical Thermodynamic Model for Si/Al Ordering in Amorphous Aluminosilicates. *Chemistry of Materials* **2005**, *17*, 2976-2986.

44.   Tran, T. T.; Bernal, S. A.; Herfort, D.; Skibsted, J. In *Characterization of the Network Structure of Alkali-Activated Aluminosilicate Binders by Single- and Double-Resonance ^{29}Si {^{27}Al} MAS NMR Experiments*, Proceedings of the 10th International Congress for Applied Mineralogy, Trondheim, Broekmans, M. A. T. M., Ed. Trondheim, 2011; pp 707-715.

45.   Andersen, M. D.; Jakobsen, H. J.; Skibsted, J., Incorporation of Aluminum in the Calcium Silicate Hydrate (C–S–H) of Hydrated Portland Cements: A High-Field ^{27}Al and ^{29}Si MAS NMR Investigation. *Inorganic chemistry* **2003**, *42*, 2280-2287.

46.   Mackenzie, K. J. D.; Smith, M. E., *Multinuclear Solid-State Nuclear Magnetic Resonance of Inorganic Materials*; Pergamon, Elsevier Science Ltd: Oxford, 2002.

47.   Houston, J. R.; Maxwell, R. S.; Carroll, S. A., Transformation of Meta-Stable Calcium Silicate Hydrates to Tobermorite: Reaction Kinetics and Molecular Structure from XRD and NMR Spectroscopy. *Geochemical Transactions* **2009**, *10*, 1-14.

48.   Pardal, X.; Brunet, F.; Charpentier, T.; Pochard, I.; Nonat, A., ^{27}Al and ^{29}Si Solid-State NMR Characterization of Calcium-Aluminosilicate-Hydrate. *Inorganic chemistry* **2012**, *51*, 1827-36.

49.   Katada, N.; Nakata, S.; Kato, S.; Kanehashi, K.; Saito, K.; Niwa, M., Detection of Active Sites for Paraffin Cracking on Usy Zeolite by ^{27}Al MQMAS NMR Operated at High Magnetic Field 16 T. *Journal of Molecular Catalysis A: Chemical* **2005**, *236*, 239-245.

50.   Malicki, N.; Mali, G.; Quoineaud, A.-A.; Bourges, P.; Simon, L. J.; Thibault-Starzyk, F.; Fernandez, C., Aluminium Triplets in Dealuminated Zeolites Detected by ^{27}Al NMR Correlation Spectroscopy. *Microporous and Mesoporous Materials* **2010**, *129*, 100-105.

51.   Richardson, I. G.; Brough, A. R.; Brydson, R.; Groves, G. W.; Dobsont, C. M., Location of Aluminum in Substituted Calcium Silicate Hydrate (C-S-H) Gels as Determined by ^{29}Si and ^{27}Al NMR and EELS. *Journal of the American Ceramic Society* **1993**, *76*, 2285-2288.

52.   Manzano, H.; Dolado, J. S.; Ayuela, A., Aluminum Incorporation to Dreierketten Silicate Chains. *The Journal of Physical Chemistry B* **2009**, *113*, 2832-2839.

53.   Manzano, H.; Dolado, J. S.; Griebel, M.; Hamaekers, J., A Molecular Dynamics Study of the Aluminosilicate Chains Structure in Al-Rich Calcium Silicate Hydrated (C–S–H) Gels. *Physica Status Solidi (A)* **2008**, *205*, 1324-1329.

54.   Bernal, S. A.; Nicolas, R. S.; Deventer, J. S. J. v.; Provis, J. L., Alkali-Activated Slag Cements Produced with a Blended Sodium Carbonate/Sodium Silicate Activator. *Advances in Cement Research* **2016**, *28*, 262-273.

55.   Bernal, S. A.; Provis, J. L.; Myers, R. J.; San Nicolas, R.; van Deventer, J. S. J., Role of Carbonates in the Chemical Evolution of Sodium Carbonate-Activated Slag Binders. *Materials and Structures* **2015**, *48*, 517-529.

56.   Loewenstein, W., The Distribution of Aluminum in the Tetrahedra of Silicates and Aluminates. *American Mineralogist* **1954**, *39*, 92-96.

57.   Faucon, P.; Delagrave, A.; Richet, C.; Marchand, J. M.; Zanni, H., Aluminum Incorporation in Calcium Silicate Hydrates (C–S–H) Depending on Their Ca/Si Ratio. *The Journal of Physical Chemistry B* **1999**, *103*, 7796-7802.

58.   Andersen, M. D.; Jakobsen, H. J.; Skibsted, J., A New Aluminium-Hydrate Species in Hydrated Portland Cements Characterized by ^{27}Al and ^{29}Si MAS NMR Spectroscopy. *Cement and Concrete Research* **2006**, *36*, 3-17.

59.   Sun, G. K.; Young, J. F.; Kirkpatrick, R. J., The Role of Al in C–S–H: NMR, XRD, and Compositional Results for Precipitated Samples. *Cement and Concrete Research* **2006**, *36*, 18-29.

60.   Taylor, R.; Richardson, I. G.; Brydson, R. M. D., Composition and Microstructure of 20-Year-Old Ordinary Portland Cement–Ground Granulated Blast-Furnace Slag Blends Containing 0 to 100% Slag. *Cement and Concrete Research* **2010**, *40*, 971-983.

61.   Wang, S. D.; Scrivener, K. L., Hydration Products of Alkali-Activated Slag Cement. *Cement and Concrete Research* **1995**, *25*, 561-571.

62.   Lothenbach, B.; Gruskovnjak, A., Hydration of Alkali-Activated Slag: Thermodynamic Modelling. *Advances in Cement Research* **2007**, *19*, 81-92.

63.   Richardson, I. G., Model Structures for C-(A)-S-H(I). *Acta Crystallographica Section B* **2014**, *70*, 903-923.

64.   Lee, S. K.; Stebbins, J. F., Extent of Intermixing among Framework Units in Silicate Glasses and Melts. *Geochimica et Cosmochimica Acta* **2002**, *66*, 303-309.

65.   Cheng, X.; Zhao, P.; Stebbins, J. F., Solid State NMR Study of Oxygen Site Exchange and Al-O-Al Site Concentration in Analcime. *American Mineralogist* **2000**, *85*, 1030.

66.   Lin, Z.; Jones, J. R.; Hanna, J. V.; Smith, M. E., A Multinuclear Solid State NMR Spectroscopic Study of the Structural Evolution of Disordered Calcium Silicate Sol-Gel Biomaterials. *Physical Chemistry Chemical Physics* **2015**, *17*, 2540-2549.

67.   Zhao, L.; Qi, Z.; Blanc, F.; Yu, G.; Wang, M.; Xue, N.; Ke, X.; Guo, X.; Ding, W.; Grey, C., Investigating Local Structure in Layered Double Hydroxides with ^{17}O NMR Spectroscopy. *Advanced Functional Materials* **2014**, *24*, 1696-1702.

68.   Viallis, H.; Faucon, P.; Petit, J. C.; Nonat, A., Interaction between Salts (NaCl, CsCl) and Calcium Silicate Hydrates (C–S–H). *Journal of Physical Chemistry B* **1999**, *103*, 5212-5219.

69.   Duxson, P.; Lukey, G. C.; Separovic, F.; van Deventer, J. S. J., Effect of Alkali Cations on Aluminum Incorporation in Geopolymeric Gels. *Ind Eng Chem Res* **2005**, *44*, 832-839.

70.   Walkley, B.; San Nicolas, R.; Sani, M. A.; Gehman, J. D.; van Deventer, J. S.; Provis, J. L., Phase Evolution of Na_2O-Al_2O_3-SiO_2-H_2O Gels in Synthetic Aluminosilicate Binders. *Dalton Transactions* **2016**, *45*, 5521-35.